JOURNAL OF BONE AND MINERAL RESEARCH
Volume 17, Number 4, 2002

Cartilage Calcification Studied by Proton Nuclear Magnetic Resonance Microscopy*

K. POTTER,[1] R.D. LEAPMAN,[2] P.J. BASSER,[3] and W.J. LANDIS[4]

ABSTRACT

A three-dimensional (3D) mineralizing culture system using hollow fiber bioreactors has been developed to study the early stages of endochondral ossification by proton nuclear magnetic resonance (NMR) microscopy. Chondrocytes harvested from the cephalic half of the sterna from 17-day-old chick embryos were terminally differentiated with 33 nM of retinoic acid for 1 week and mineralization was initiated by the addition of 1% β-glycerophosphate to the culture medium. Histological sections taken after 6 weeks of development in culture confirmed calcification of the cartilage matrix formed in bioreactors. Calcium to phosphorus ratios (1.62–1.68) from X-ray microanalysis supported electron diffraction of thin tissue sections showing the presence of a poorly crystalline hydroxyapatite mineral phase in the cultures. After 4 weeks of culture, quantitative proton NMR images showed water proton magnetization transfer rate constants (k_m) were higher in premineralized cartilage compared with uncalcified cartilage, a result suggesting collagen enrichment of the matrix. Notably after 5 weeks mineral deposits formed in bioreactors principally in the collagen-enriched zones of the cartilage with increased k_m values. This caused marked reductions in water proton longitudinal (T_1) and transverse (T_2) relaxation times and water diffusion coefficients (D). These results support the hypothesis that mineralization proceeds in association with a collagen template. After 6 weeks of culture development, the water proton T_2 values decreased by 13% and D increased by 7% in uncalcified areas, compared with the same regions of tissue examined 1 week earlier. These changes could be attributed to the formation of small mineral inclusions in the cartilage, possibly mediated by matrix vesicles, which may play an important role in cartilage calcification. In summary, NMR images acquired before and after the onset of mineralization of the same tissue provide unique insights into the matrix events leading to endochondral mineral formation. (J Bone Miner Res 2002;17:652–660)

Key words: nuclear magnetic resonance microscopy, cartilage, calcification, chondrocyte, bioreactor

INTRODUCTION

THE EARLY detection of mineral deposits and the characterization of the inorganic solid phases of calcium phosphate in bone and other calcified vertebrate tissues are critical for understanding changes in mineralized tissues attributable to normal growth and development, therapeutic interventions, or disease pathologies.[1] The identity of the earliest mineral phases deposited in these tissues is still uncertain because the phases may be transient or changes in equilibrium concentrations of critical ions during tissue processing may result in changes in the phase and composition of the mineral.[2] The application of proton nuclear magnetic resonance (NMR) microscopy now makes it pos-

*Published abstract appears in Proc Int Soc Magn Reson Med 2001;9:2126.

The authors have no conflict of interest.

[1]Department of Cellular Pathology and Genetics, Armed Forces Institute of Pathology, Washington, DC, USA.
[2]Supramolecular Structure and Function Resource, Office of Research Services, National Institutes of Health, Bethesda, Maryland, USA.
[3]Section on Tissue Biophysics and Biomimetics, National Institute of Child Health and Human Development, Bethesda, Maryland, USA.
[4]Department of Biochemistry and Molecular Pathology, Northeastern Ohio Universities College of Medicine, Rootstown, Ohio, USA.

sible to circumvent some of these difficulties and to examine both the organic and the inorganic phases of calcified tissues by noninvasive means and without fixation, destructive sectioning, or histological staining.[3]

This study was motivated by the need for a rapid bioanalytical technique that can assess the mineralization of long bones and the process of endochondral ossification. At present, the approaches to many analyses of the time course of bone formation and remodeling demand that bones be harvested at different time points and subjected to invasive techniques such as dissection, fixation, sectioning, staining, or other procedures required for histomorphometry, electron diffraction, and scanning and transmission electron microscopy (TEM). Noninvasive X-ray–based techniques that avoid some of these procedures are limited by the fact that little contrast difference may be detected between newly formed and progressively more mature bone.

Proton NMR offers a novel noninvasive approach for investigating mineralized tissues.[3,4] Although proton NMR images of bone yield very little signal, investigators have successfully assessed trabecular architecture and hence strength and fracture risk of cancellous bone using the high-intensity signal from the intervening bone marrow.[5–8] A few groups also have applied solid-state imaging techniques to detect phosphorus-31 nuclei immobilized in the inorganic matrix of bone.[9–11] In this work, proton NMR imaging has been used to examine bone formation de novo in a mineralizing cell culture system. Small calcified deposits do not result in a complete loss of signal and thereby provide a unique opportunity to relate water proton NMR properties to mineral quantity and quality.

For this study a three-dimensional (3D) mineralizing cell culture system based on an NMR-compatible hollow fiber bioreactor (HFBR) has been developed.[12–14] The system models the process of endochondral ossification of a long bone in which cartilage matrix, elaborated around the hollow fibers, mineralizes. Over a 6-week period, the growth and eventual mineralization of the cartilage in this system have been studied spatially and temporally with proton NMR microscopy, and various NMR parameters have been measured and correlated with the regions of mineral formation imaged by this technique. After 6 weeks of culture, all samples were processed histologically and ultrastructurally to determine the spatial location of putative mineral deposits and associated matrix components. The formation of an apatitic mineral phase in the tissue developed in this bioreactor system was verified using X-ray spectroscopy and electron diffraction.

MATERIALS AND METHODS

Bioreactor inoculation

The bioreactor was constructed from high-purity glass tubing (inner diameter, 4 mm; length, 60 mm) with a side-port for the introduction of cells. Inside each bioreactor were six porous polypropylene hollow fibers (inner diameter, 330 μm; 0.2-μm pores; Microgon, Inc., Laguna Hills, CA, USA) embedded in biomedical grade silicon rubber (MED-1137; NuSil Silicone Technology, Carpinteria, CA, USA).

Cell populations rich in mature hypertrophic chondrocytes were isolated from the cephalic halves of 17-day-old chick embryo sterna. Sterna were digested with 4 mg/ml collagenase (Roche Molecular Biochemicals, Indianapolis, IN, USA) for 3 h at 37°C with agitation.[15,16] Isolated chondrocytes were resuspended in tissue culture medium and 3×10^7 cells were injected through the side-port into the extracapillary space of the bioreactor. Two hours after inoculation of bioreactors with chondrocytes, perfusion with tissue culture medium was initiated using a pin compression pump (Cellco, Germantown, MD, USA) maintained in a 5% CO_2 incubator.

Tissue culture medium was prepared by adding 10 ml of heat-inactivated fetal bovine serum (Biofluids, Rockville, MD, USA), 5 ml of 200 mM L-glutamine (Biofluids), 0.5 ml of 250 μg/ml of fungizone (Biofluids), and 0.5 ml of 10 mg/ml of gentamicin reagent solution (Gibco BRL, Gaithersburg, MD, USA) to a 500-ml bottle of Dulbecco's modified Eagle's medium (Biofluids). Ascorbic acid (Sigma, St. Louis, MO, USA) was added at each medium change, twice per week, such that its final concentration was 10 μg/ml.

Mineralization was initiated by dosing each bioreactor with 33 nM of all-*trans*-retinoic acid (Sigma) for 1 week after 3 weeks of growth.[17,18] After retinoic acid treatment, the tissue culture medium was supplemented with 1% β-glycerophosphate (Sigma) and 50 μg/ml of ascorbic acid to facilitate mineral formation.

Proton NMR microscopy

All NMR microscopy experiments were performed on a Varian Inova spectrometer (Varian, Palo Alto, CA, USA) coupled to a 4.7-T magnet (200.6 MHz for ^{1}H). The radiofrequency probe (rf) consisted of a three-turn solenoid coil wrapped around individual bioreactors. The probe was inserted into a radiofrequency resonant circuit. The imaging plane was perpendicular to the long axis of the bioreactor and was located ~5 mm from the outflow end. A field-of-view of 8 mm, a slice thickness of 2 mm, and a matrix size of 128×128, yielding a nominal in-plane resolution of 62 μm, were used. Throughout data acquisition, bioreactors were maintained under incubator-like conditions (37°C and 5% CO_2). Measurements were made of the water proton longitudinal (T_1) and transverse (T_2) relaxation times, the magnetization transfer rate (k_m) constant, and the water diffusion coefficient (D) at 4, 5, and 6 weeks postinoculation of chondrocytes into the bioreactors.

T_1 maps were obtained from a series of 2D spin-echo images using a repeat time (TR) ranging between 0.2 and 5 s, with a fixed echo time (TE) of 12.5 ms. T_2 maps were calculated from images acquired with TE ranging from 0.0125 to 0.112 s, with TR fixed at 5 s. Water diffusion maps were calculated from a series of images acquired with the pulsed-gradient spin-echo (PGSE) sequence in which gradients values ranged from 1 to 9 gauss/cm.[19] Typical values for the diffusion (Δ) and gradient duration (δ) times were 20 ms and 10 ms, respectively.

The k_m values at each pixel were calculated from a series of images acquired with a 12-μT saturation pulse applied 6000 Hz off-resonance, with varying saturation times (t_p = 0.1–4 s), before a standard spin-echo imaging sequence.[20] The observed image intensity $M_s(t_p)$ after the application of a saturation pulse of length t_p was fit according to the expression $M_s(t_p) = (M_o - M_{so}) \exp(-t_p/T_{1sat}) + M_{so}$. The k_m map was calculated according to $k_m = [1 - M_{so}/M_o]/T_{1sat}$, where M_{so}/M_o is defined as the ratio of image intensities acquired with and without the application of an infinitely long saturation pulse. T_{1sat} is defined as the longitudinal relaxation time of the free protons in the presence of an off-resonance saturation pulse.

Image analysis was performed off-line with user-defined procedures in Interactive Data Language (IDL; Research Systems, Inc., Boulder, CO, USA). End-stage NMR images, with defined mineralized zones, were used to determine regions of calcifying and noncalcifying cartilage in early stage images. NMR values for calcifying and noncalcifying cartilage are reported as the mean ± SD of the pixel values in that region of interest.

Histology

After NMR imaging, the intact tissue with its complement of hollow fibers was removed from glass bioreactors and fixed in neutral buffered formalin for 2 days at 4°C. Then, the tissue and fibers were embedded in paraffin and sectioned (~5 μm thickness) perpendicular to the long axis of the bioreactor. Sections were stained with Alcian blue (pH 2.5) and Masson's trichrome for detection of sulfated proteoglycan (PG; blue color) and collagen (blue), respectively.[21] The spatial distribution of mineral deposits was determined by comparing similar sections stained with von Kossa and alizarin red, which localized phosphate (black) and calcium (red), respectively.[21]

Mineral characterization

Some bioreactor contents were processed in ethylene glycol (Sigma) and embedded in LR white resin (EF Fullam, Inc., Latham, NY, USA), thin-sectioned (~80 nm) on a Reichert Ultracut S ultramicrotome (Leica, Deerfield, IL, USA), floated briefly on a microtome trough of double-distilled water (pH > 8), mounted on copper grids, and left unstained.[22] Thin sections were examined by electron microscopy at a beam voltage of 120 kV in a CM120 transmission electron microscope (FEI, Eindhoven, The Netherlands) equipped with an Oxford Pentafet energy-dispersive X-ray detector (Oxford Instruments, High Wycombe, UK) and a GIF100 imaging filter (Gatan, Inc., Pleasanton, CA, USA).[23] After observation and image recording, small mineral deposits were examined by selected area electron diffraction (SAED) from 1-μm-diameter areas of the specimen. Diffraction patterns were energy-filtered to exclude all but zero-loss electrons. This method removed background intensity caused by multiply scattered electrons[24] and was especially important for diffraction patterns recorded from thicker regions of the specimens. A grid of evaporated gold (EF Fullam, Inc.) was used to calibrate the camera length of the microscope in diffraction. Diffraction patterns and images were recorded digitally using a cooled charge coupled device (CCD) array camera that was controlled by Gatan Digital Micrograph v. 3.3 software (Gatan, Inc.) running on a Power Macintosh computer. Diffraction data were read into the National Institutes of Health (NIH) IMAGE program available from Wayne Rasband at the NIH (http://rsb.info.nih.gov/nih-image/)[25] to measure the diameters of observed polycrystalline ring patterns. After collection of the diffraction data, the electron beam was focused to a diameter of ~0.5 μm onto the same mineral deposits examined by SAED and energy-dispersive X-ray spectra were acquired for times between 50 and 100 s. Quantitative microanalysis was performed using the NIST/National Institutes of Health Desktop Spectrum Analyzer (DTSA).[26] Peak areas of emission lines quantitated by simplex curve fitting and atomic ratios of Ca/P were obtained from the calculated relative efficiency factors for Ca and P X-ray production and detection. The DTSA program determines such efficiency factors from the known detector parameters entered by the operator and by modeling the physics of X-ray generation in the specimen.

RESULTS

Histology

Representative histological sections through mineralized cartilage tissue obtained from a HFBR 6 weeks postinoculation are shown in Fig. 1. Sections were initially cut perpendicular to the long axis of the bioreactor and the resulting transverse sections of the hollow fibers show the tissue formed in extracapillary spaces. Tissue sections were treated with von Kossa (Fig. 1A), alizarin red (Fig. 1B), Alcian blue (Fig. 1C), and Masson's trichrome (Fig. 1D) stains.

Von Kossa staining (Fig. 1A) does not distinguish between the presence of organic and inorganic phosphates here; both sites appear black in tissue sections. Inorganic phosphate is associated with the location of mineral deposits. Because von Kossa alone does not define mineral sites, counterpart tissue sections were treated with alizarin red, a stain for calcium (Fig. 1B). Those regions staining for both phosphate by von Kossa and calcium by alizarin red were identified as calcified cartilage. Mineralized zones with von Kossa and alizarin red staining were not precisely superimposable because of slice-to-slice variability between tissue sections.

By Alcian blue staining (Fig. 1C), the bioreactor-derived tissue was histologically similar to hyaline cartilage as evidenced by chondrocytes in well-defined lacunae surrounded by a metachromatic matrix. However, the tissue was not uniformly stained and reduced Alcian blue staining intensity was observed in mineralized areas, whereas the matrix adjacent to the hollow fibers in the bioreactor was intensely basophilic. This appearance was in contrast to that resulting from cartilage treated with Masson's trichrome (Fig. 1D). In this case, the intensity of Masson staining in mineralized zones of the culture tissue and hence its collagen content were increased.

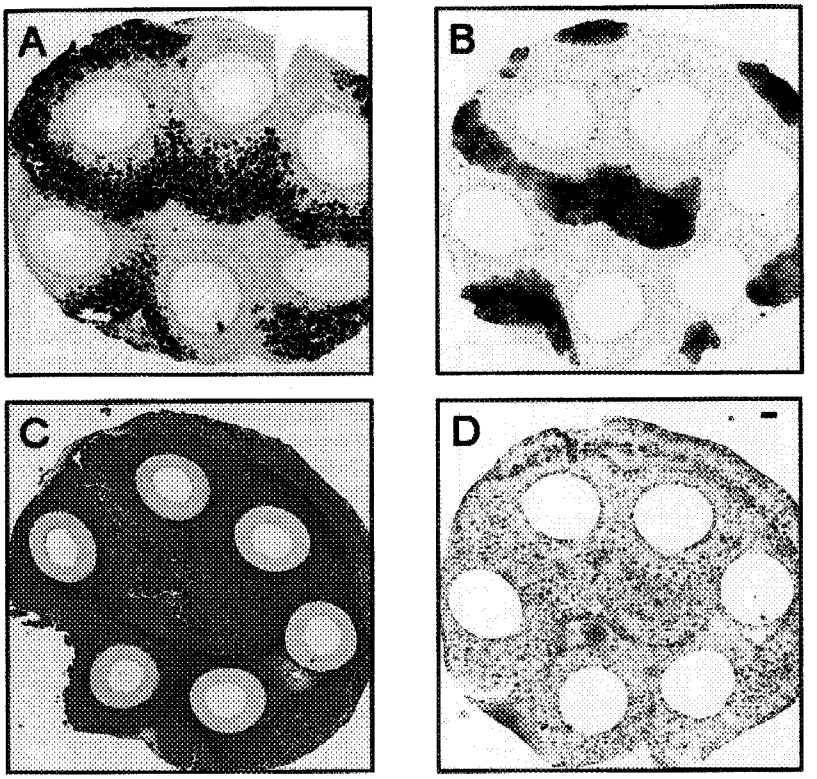

FIG. 1. Histological sections of bioreactor-derived cartilage cut perpendicular to the hollow fiber axis. Six hollow fibers are shown in cross-section. Tissue sections were stained with (A) von Kossa (black, phosphate), (B) alizarin red (red, calcium), (C) Alcian blue (blue, PGs), and (D) Masson's trichrome (blue, collagen). Sections were obtained from the same tissue 6 weeks after inoculation with chondrocytes (bar = 100 μm).

Mineral characterization

The presence and crystallographic nature of mineral deposits were studied in the bioreactor-derived cartilage. Tissue sections, prepared using anhydrous techniques to maintain mineral intrinsic to the tissue, were examined unstained by TEM, SAED, and X-ray microanalysis. Dark regions in TEM images (Fig. 2A) represent mineral deposits, and translucent regions are uncalcified organic matrix regions of cartilage. A representative electron diffraction pattern from the mineralized site indicated in Fig. 2A is shown in Fig. 2B. The diffraction pattern consists of two principal rings, an inner weaker reflection corresponding to the 002 plane of hydroxyapatite and an outer stronger reflection corresponding to the coincident reflections of the 211, 112, and 300 planes of hydroxyapatite. This pattern confirms that the mineral produced in these bioreactor cultures is that of poorly crystalline hydroxyapatite, which is typical of the form found in newly developing cartilage and bone of vertebrate mineralizing tissues.[22,27]

Energy-dispersive X-ray spectra were acquired from approximately the same regions examined by electron diffraction. The largest peaks observed over mineralized and unmineralized cartilage were those of carbon and oxygen. Mineralized regions of the tissue (Fig. 2C) also yielded phosphorus ($K\alpha$ = 2.0 keV) and calcium ($K\alpha$ = 3.7 keV and $K\beta$ = 4.0 keV) signals. The Ca/P ratios, after integrating the areas under the respective peaks, were 1.62–1.68 (n = 4). These values are comparable with published Ca/P ratios of synthetic hydroxyapatite.[28] An X-ray spectrum from the organic matrix of the cartilage is shown in Fig. 2D. Relatively small signals of phosphorus and calcium and greater peaks of sodium ($K\alpha$ = 1.0 keV) and sulfur ($K\alpha$ = 2.3 keV) were detected over this and similar uncalcified regions of the tissue. The latter elements arise most likely from the presence of sulfated PGs and sodium counterions in the tissue.[29]

Proton NMR microscopy

Signals unique to NMR microscopy were measured for mineralizing bioreactors to compare with data obtained from histology and analytical electron microscopic methods. A series of representative NMR images is shown in Fig. 3 and was acquired at the same location within a single bioreactor 4, 5, and 6 weeks after inoculation with chondrocytes. At weekly intervals, water proton longitudinal (T_1) and transverse (T_2) relaxation times, water diffusion coefficient (D), and magnetization transfer rate (k_m) were determined. Each image of Fig. 3 represents a 2-mm slice of tissue taken perpendicular to the long axis of the bioreactor, with a nominal in-plane resolution of 62 μm. The NMR properties of calcifying and noncalcifying tissue were extracted from NMR images using regional templates generated from end-stage NMR images and the results are summarized as a series of bar graphs in Fig. 4.

According to the NMR images in Fig. 3, the culture medium in the fiber lumen had the highest values (brightest regions of image) in T_1, T_2, and diffusion maps, consistent with the fast molecular motions and free diffusivity of water protons in the medium. The k_m map shows the medium to be

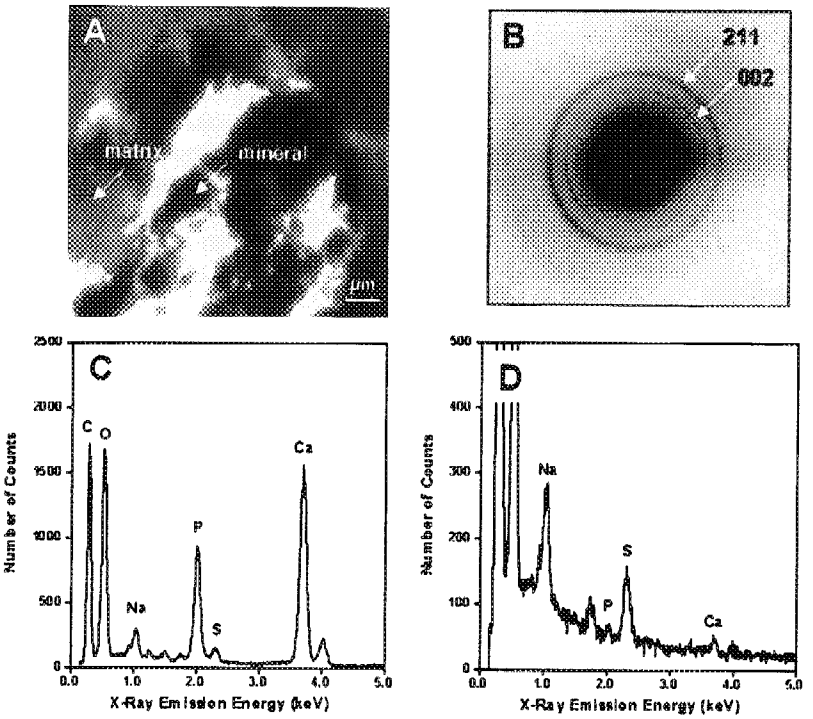

FIG. 2. (A) Transmission electron micrograph of a portion of calcified cartilage prepared using anhydrous techniques, sectioned (~80 nm thick), and left unstained. Mineralized zones appear dark and uncalcified zones appear translucent in the TEM image (bar = 1 μm). (B) Selected area diffraction pattern (120 kV) of mineral deposit indicated by the arrow on TEM image. Reflections are indicative of poorly crystalline hydroxyapatite. (C and D) X-ray energy spectra of calcified and uncalcified matrix, respectively, from sites in panel A. Carbon and oxygen are prominent peaks in both spectra. (C) Phosphorus and calcium dominate the region of mineralized cartilage and (D) sodium and sulfur are found in uncalcified matrix. Note the scale difference in peak counts between panel C and D.

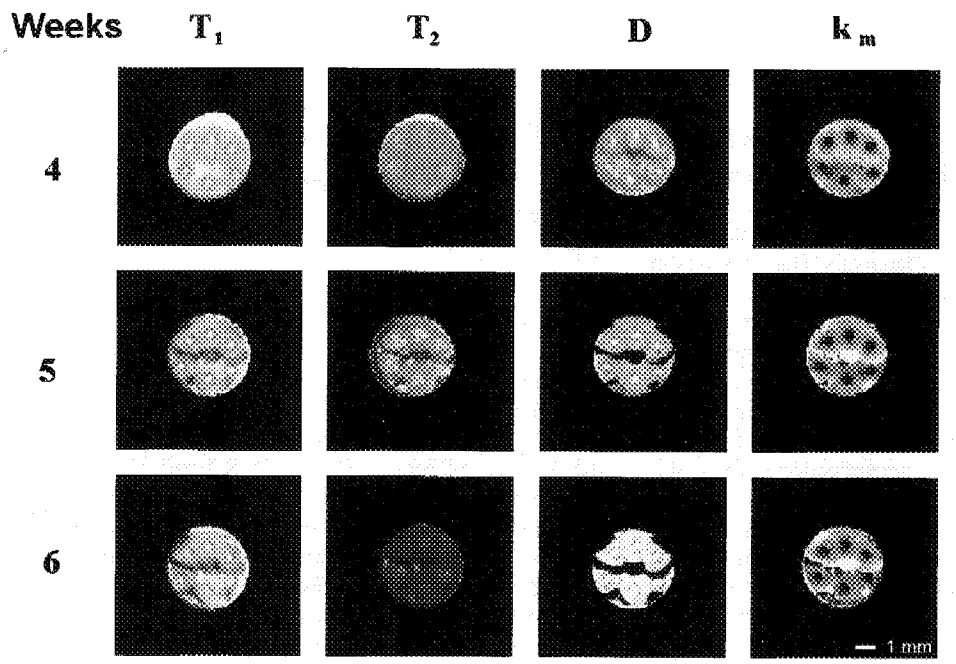

FIG. 3. Quantitative water proton T_1, T_2, D, and k_m maps of a mineralizing bioreactor at 4, 5, and 6 weeks postinoculation. The image plane was oriented perpendicular to the hollow fiber axis, thereby showing the culture medium in the fiber lumen. Slice thickness was 2 mm and the nominal in-plane resolution was 62 μm (bar = 1 mm).

dark, a result of it containing fewer macromolecules than the cartilage tissue surrounding the fibers.

The water proton T_1 value for noncalcifying cartilage (Fig. 4A) was found to be 2.54 ± 0.30 s at week 4 and only slightly lower at weeks 5 and 6 (2.33 ± 0.30 s). This was in contrast to data from calcifying cartilage in which the water proton T_1 value at week 4 (2.43 ± 0.30 s) was significantly lower at week 5 (1.71 ± 0.29 s). The mean T_1 value of calcifying cartilage at week 6 was comparable with that for week 5 despite the marked heterogeneity observed in the T_1 map shown in Fig. 3.

The T_2 map of the cartilage tissue before mineralization at week 4 was relatively homogeneous. There was no measurable difference in the T_2 values (Fig. 4B) of calcifying and noncalcifying cartilage (32 ± 2 ms). However, by week 5 the water proton T_2 value of calcifying cartilage was significantly reduced (25 ± 7 ms) compared with noncalcifying cartilage (34 ± 6 ms). Notably, at week 6 the T_2 of

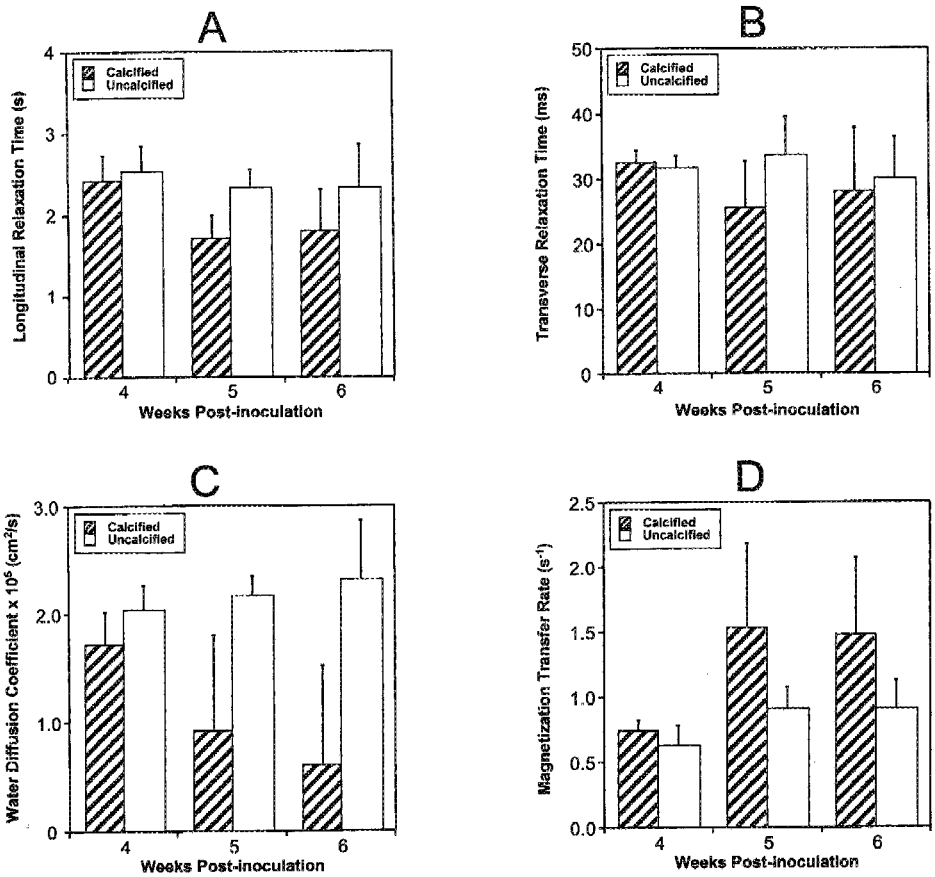

FIG. 4. Bar graphs of the water proton (A) T_1, (B) T_2, (C) D, and (D) k_m values for calcifying (hatched) and noncalcifying (white) cartilage within a single bioreactor at 4, 5, and 6 weeks postinoculation. Values correspond to the mean ± pixel SD of calcifying and noncalcifying cartilage zones, defined by end-stage NMR images.

noncalcifying cartilage was significantly reduced (30 ± 6 ms) compared with the same tissue at week 5.

The water diffusion map at week 4 was mostly homogeneous (2.04 ± 0.22 × 10^{-5} cm^2/s) except for a dark premineralized zone (1.72 ± 0.30 × 10^{-5} cm^2/s). After 5 weeks, calcified cartilage zones were devoid of signal because the TE used in the PGSE sequence was relatively long (40 ms) compared with the T_2 values in this zone. Thus, water diffusion values in the presence of mineral could not be measured, thereby reducing the average diffusion value reported for calcified cartilage in Fig. 4C. It is clear from the diffusion maps presented in Fig. 3 that the size of the mineralized zone had increased from weeks 5 to 6. Notably, the diffusion coefficient of water in the noncalcifying cartilage was higher at week 6 (2.32 ± 0.55 × 10^{-5} cm^2/s) compared with week 5 (2.17 ± 0.18 × 10^{-5} cm^2/s).

The k_m maps presented in Fig. 3 give the rate of exchange between free water and macromolecule-associated water. Thus, in the presence of collagen, the measured k_m value for water protons is high. For noncalcifying cartilage, k_m increased from 0.63 ± 0.15 s^{-1} at week 4 to 0.90 ± 0.2 s^{-1} at week 6 (Fig. 4D). This was in contrast to the k_m values for calcifying cartilage, which increased from 0.73 ± 0.09 s^{-1} at week 4 to 1.53 ± 0.65 s^{-1} at week 5. The k_m value for calcified cartilage at week 6 (1.47 ± 0.6 s^{-1}) was slightly reduced because of a reduced signal in high mineral containing regions.

DISCUSSION

The development of an NMR-compatible cartilage mineralizing culture system has made it possible to monitor noninvasively a sequence of biological and physicochemical events that describes the endochondral ossification process common to vertebrate calcifying tissues. This isolated cell culture system has facilitated the measurement of water proton NMR properties unique to calcifying and noncalcifying cartilage. It has yielded insights into events governing compositional changes of the organic matrix of the tissue in its preparation for mineralization. The data presented here are an extension of results obtained previously with the same HFBR system.[12–14] The principal limitation of this system is that calcified cartilage does not remodel through subsequent stages leading to woven or lamellar bone.

Despite this shortcoming, it is clear that early mineralization of cartilage can be supported by this bioreactor system and that mineral formation can be detected and followed in the absence of cell types other than chondrocytes and without the addition to the medium of numerous exogenous factors. Inoculation of bioreactors with a population of cells rich only in hypertrophic chondrocytes produces a cartilage matrix that ultimately mineralizes. The cells were terminally differentiated with retinoic acid, which induces late maturation genes and activates the mineralization of the cartilage matrix.[17,18] Ascorbic acid and

β-glycerophosphate were added to aid in collagen and mineral formation.[15,16]

Conventional histological sections of the cartilage tissue developed in the bioreactor culture clearly reveal the presence and distribution of mineral deposits formed in this system. Mineralized zones were unambiguously identified in those regions that were commonly made apparent by both alizarin red and von Kossa staining. Differences in the extent and pattern of mineral formation by the two stains separately applied are most likely the result of slice-to-slice variation in mineral deposition. Staining differences with von Kossa also could be explained by variation in the accumulation of phosphates (both organic and inorganic) in the extracellular matrix of the cartilage before mineralization. It also is conceivable that exposure to water during alizarin red staining washed away some labile calcium salts within the section and thereby reduced the degree of apparent calcification.

In the calcified cartilage zones of the tissues, the reduction in Alcian blue staining intensity can be attributed to a reduction in matrix PGs as well as to an increase in the number of large hypertrophic chondrocytes comprising this region of the cartilage. The increase in the Masson's trichrome staining intensity for the same zones reflects an increase in the collagen content of the zones as well as a putative unmasking of collagen owing to reduced quantities of PG. These histological results obtained for the bioreactor system are consistent with the understanding from other studies in vivo and in vitro that both collagen and PGs play an important role in regulating the mineralization process.[1,30]

Histological stains give no information about the crystallographic nature or elemental composition of the mineral that is deposited in these bioreactor cultures. Thus, to characterize the mineral as apatitic, electron optical and analytical methods were used in combination with anhydrous techniques of tissue preparation.[22,28,31] The latter avoids possible changes in mineral phase and/or composition.[22] This approach yielded Ca/P ratios from X-ray microanalysis of 1.62–1.68, values consistent with the literature for synthetic hydroxyapatite.[28] Ca/P ratios alone cannot be used to identify a particular mineral phase because a single phase may yield a range of ratios. Conclusive identification of an apatitic mineral in the thin sections examined was obtained by SAED. Diffraction reflections from the bioreactor samples were those of poorly crystalline hydroxyapatite on comparison with known crystal structure data obtained from Mincryst (http://database.iem.ac.ru/mincryst/s_carta.php3?231/).

The NMR images presented in this study clearly reveal the spatial and temporal changes in both the organic and the inorganic matrices of cartilage tissue undergoing an endochondral process of mineralization. Premineralized cartilage in the early stages of its transition to mineralized cartilage was located using calcified cartilage templates from end-stage NMR images, providing unique NMR properties of the organic matrix before mineralization. The main limitation of the technique is its inability to resolve individual cells or mineral deposits. Instead, it measures the net change in composition of the tissue contained within an imaging voxel.

It should be noted that measurements derived from 2D slice experiments in which the slice thickness is much greater than a cell diameter would have significant volume averaging in the slice direction. If axial symmetry is assumed for the bioreactor system, then volume averaging in the axial (slice) direction will not affect the findings of this work, especially because much of the tissue variation occurs radially outward from the fibers. Another alternative would be to map the entire region inside the sensitive volume of the rf coil in 3D. The advantage here is that imaging voxels will be comparable with the size of a cell. However, a single 3D volume image would require a longer acquisition time than a 2D slice image. Hence, the experimental time needed to extract quantitative NMR parameters in three dimensions would be prohibitive. For the most part, the image intensity of a 3D data set represents a weighted function of tissue NMR properties and acquisition parameters, which is difficult to interpret in terms of tissue constituents.

The earliest evidence of mineral formation was apparent in water proton diffusion maps of cartilage 4 weeks after inoculation of bioreactors with chondrocytes. Cartilage regions undergoing calcification, exemplified by reduced D values at week 4, are characterized by low D values that further decrease as mineralization proceeds. The observed reduction in D occurs before a detectable change in both water proton T_1 and water proton T_2 values for the same cartilage zones 4 weeks after cell inoculation. This result indicates that water in these zones is rotationally mobile but shows reduced translational mobility. Similar NMR results have been reported for solutions of cartilage PGs in the presence of 100 mM of $CaCl_2$.[32] In this case, it was speculated that calcium induced a structural transition in the PGs, which are thought to play a role in the calcification process.[32] Such a putative calcium-induced collapse of PGs in premineralized cartilage zones could result in the unmasking of collagen fibers, an event that would effectively increase the amount of collagen available to interact with water molecules. An increase in collagen content of this nature could explain the increase in k_m values observed here in premineralized zones compared with surrounding tissue, a result consistent with literature reports in which higher k_m values imply a higher tissue collagen content.[13,14,33,34]

At week 5, both T_1 and T_2 maps clearly reveal the mineralized zones within the cartilage matrix as low intensity zones. However, water proton T_1 values were not uniformly reduced throughout these zones. T_1 values were the lowest in those zones that contained sufficient mineral to alter the mobility of the surrounding water molecules.[35] This is consistent with NMR relaxation studies of water in the presence of different calcium salts.[36,37] In some areas of the cartilage matrix, T_1 was only slightly higher than those regions with the lowest T_1 values. This may be the result of reduced amounts of mineral or a change in mineral composition in such regions. T_2 values in the mineralized zones were uniformly reduced because this parameter is very sensitive to susceptibility gradients generated by even the smallest mineral deposits. In the water diffusion maps obtained here, calcified cartilage zones appear as regions devoid of signal because the echo time of diffusion exper-

iments is longer than the T_2 of water in mineralized zones. Thus, diffusion maps provide little information about mineral quantity or quality, although they provide a general measure of the extent of mineralization.

In regions of cartilage producing the lowest T_1 and T_2 values, k_m values were highest. This result can be attributed to reduced water and increased collagen content of the calcified cartilage compared with uncalcified cartilage. These data also are consistent with high k_m values measured for periosteal bone, as compared with the cartilage matrix, in the avian growth plate.[3] The k_m parameter is especially valuable because it provides information about the state of the collagen fibers throughout the mineralization process. Importantly, k_m results support the notion that collagen enrichment is a prerequisite for mineralization.

The region of cartilage calcification in bioreactors increased from week 5 to 6. During this period, changes in the NMR properties of the surrounding uncalcified cartilage were apparent also. These included the observations that the cartilage T_2 values decreased and water diffusion coefficients increased compared with values measured for the same tissue a week earlier. The decrease in T_2 possibly reflects the formation of small mineral deposits throughout the organic matrix. These deposits will have little effect on water mobility, so they subsequently will have little effect on T_1. However, as discussed earlier, such small deposits will attenuate water proton T_2 values because of significant susceptibility gradients that arise with the sudden presence of a solid-liquid interface where none existed before. The susceptibility gradients will cause enhanced diffusion attenuation for the same applied gradients in the PGSE experiment, resulting in an apparent increase in water mobility. These observations together suggest that there are many small mineralization sites throughout the cartilage tissue. On the other hand, histology does not reveal them. One explanation of this fact is that the aqueous preparation techniques disrupt small and presumably labile mineral phases comprising such deposits. Histology also may be of insufficient resolution to reveal them. Possibly the deposits are mediated by matrix vesicles at this stage of cartilage development[38] and such vesicles can be observed not by histology but by electron microscopy. Owing to its nondestructive nature and in view of the present results, NMR can provide valuable insights concerning the onset of mineral deposition in cartilage. Finally, concerning calcified cartilage zones having no detectable signals even in k_m maps, the observed signal loss could result from mineralization proceeding until the mineral invades fluid-filled chondrocyte lacunae to form dense mineral deposits.

In summary, this study introduces a 3D tissue model for studying endochondral ossification based on a HFBR. The advantage of this model system over ex vivo samples is that changes in the NMR signal intensity can be attributed to mineral deposition rather than the presence of hematopoietic cells of the marrow or invading blood vessels. This NMR-compatible tissue model provides a unique means whereby the events underlying endochondral ossification can be followed noninvasively and the NMR parameters can be correlated precisely with spatial characteristics defined by histology. Once suitable NMR measurements have been developed for monitoring bone formation in vitro, this system could be used to assess the efficacy of therapeutic or pathological interventions on bone formation with each system acting as its own control. Finally, the NMR technique can be applied to bone formation studies in vivo.

ACKNOWLEDGMENTS

The authors thank Dr. Iren Horkay (National Institute of Child Health and Human Development) for her assistance with the cell isolation procedure and Jennifer Hillyer (Northeastern Ohio Universities College of Medicine) for the preparation of tissue samples for TEM studies. The authors are also grateful to Dr. William Swaim (National Institute of Dental and Craniofacial Research) for help with histology and to Scott Chesnick (National Heart, Lung, and Blood Institute) for design and fabrication of the radiofrequency probe used for NMR imaging experiments.

REFERENCES

1. Christoffersen J, Landis WJ 1991 A contribution with review to the description of mineralization of bone and other calcified tissues in vivo. Anat Rec **230:**435–450.
2. Boskey AL 1998 Biomineralization: Conflicts, challenges, and opportunities. J Cell Biochem Suppl **31:**83–91.
3. Potter K, Landis WJ, Spencer RGS 2001 Histomorphometry of the embryonic avian growth plate by proton nuclear magnetic resonance microscopy. J Bone Miner Res **16:**1092–1100.
4. Matteson SR, Deahl ST, Alder ME, Nummikoski PV 1996 Advanced imaging methods. Crit Rev Oral Biol Med **7:**346–395.
5. Chung HW, Wehrli FW, Williams JL, Wehrli SL 1995 Three-dimensional nuclear magnetic resonance microimaging of trabecular bone. J Bone Miner Res **10:**1452–1461.
6. Ouyang X, Selby K, Lang P, Engelke K, Klifa C, Fan B, Zucconi F, Hottya G, Chen M, Majumdar S, Genant HK 1997 High resolution magnetic resonance imaging of the calcaneus: Age-related changes in trabecular structure and comparison with dual X-ray absorptiometry measurements. Calcif Tissue Int **60:**139–147.
7. Majumdar S, Kothari M, Augat P, Newitt DC, Link TM, Lin JC, Lang T, Lu Y, Genant HK 1998 High-resolution magnetic resonance imaging: Three-dimensional trabecular bone architecture and biomechanical properties. Bone **22:**445–454.
8. Majumdar S, Newitt D, Mathur A, Osman D, Gies A, Chiu E, Lotz J, Kinney J, Genant H 1996 Magnetic resonance imaging of trabecular bone structure in the distal radius: Relationship with X-ray tomographic microscopy and biomechanics. Osteoporos Int **6:**376–385.
9. Ackerman JL, Raleigh DP, Glimcher MJ 1992 Phosphorus-31 magnetic resonance imaging of hydroxyapatite: A model for bone imaging. Magn Reson Med **25:**1–11.
10. Moore JR, Garrido L, Ackerman JL 1995 Solid state phosphorus-31 magnetic resonance imaging of bone mineral. Magn Reson Med **33:**293–299.
11. Wu Y, Ackerman JL, Chesler DA, Li J, Neer RM, Wang J, Glimcher MJ 1998 Evaluation of bone mineral density using three-dimensional solid state phosphorus-31 NMR projection imaging. Calcif Tissue Int **62:**512–518.
12. Petersen E, Potter K, Butler J, Fishbein KW, Horton WE, Spencer RGS, McFarland EW 1997 Bioreactor and probe system for magnetic resonance microimaging and spectroscopy of chondrocytes and neocartilage. Int J Imaging Syst Tech **8:**285–292.

13. Potter K, Butler JJ, Adams C, Fishbein KW, McFarland EW, Horton WE, Spencer RG 1998 Cartilage formation in a hollow fiber bioreactor studied by proton magnetic resonance microscopy. Matrix Biol **17:**513–523.
14. Potter K, Butler J, Horton WE, Spencer RGS 2000 Response of engineered cartilage tissue to biochemical agents as studied by proton MRI microscopy. Arthritis Rheum **43:**1580–1590.
15. Horton W, Hassell JR 1986 Independence of cell shape and loss of cartilage matrix production during retinoic acid treatment of cultured chondrocytes. Dev Biol **115:**392–397.
16. Gerstenfeld LC, Landis WJ 1991 Gene expression and extracellular matrix ultrastructure of a mineralizing chondrocyte cell culture system. J Cell Biol **112:**501–513.
17. Iwamoto M, Shapiro IM, Yagami K, Boskey AL, Leboy PS, Adams SL, Pacifici M 1993 Retinoic acid induces rapid mineralization and expression of mineralization-related genes in chondrocytes. Exp Cell Res **207:**413–420.
18. Iwamoto M, Yagami K, Shapiro IM, Leboy PS, Adams SL, Pacifici M 1994 Retinoic acid is a major regulator of chondrocyte maturation and matrix mineralization. Microsc Res Tech **28:**483–491.
19. Stejskal EO, Tanner JE 1965 Spin diffusion measurements: Spin echoes in the presence of a time-dependent field gradient. J Chem Phys **42:**288–292.
20. Hajnal JV, Baudouin CJ, Oatridge A, Young IR, Bydder GM 1992 Design and implementation of magnetization transfer pulse sequences for clinical use. J Comp Assist Tomogr **16:** 7–18.
21. Prophet EB, Mills B, Arrington JA, Sobin LH (eds.) 1992 Laboratory Methods in Histotechnology. American Registry of Pathology, Washington, DC.
22. Landis WJ, Glimcher MJ 1978 Electron diffraction and electron probe microanalysis of the mineral phase of bone tissue prepared by anhydrous techniques. J Ultrastruct Res **63:**188–223.
23. Krivanek OL, Friedman SL, Gubbens AJ, Kraus B 1995 An imaging filter for biological applications. Ultramicroscopy **59:** 267–282.
24. Mayer J, Deininger C, Reimer L 1995 Electron spectroscopic diffraction. In: Reimer L (ed.) Transmission Electron Microscopy, vol. 71. Springer-Verlag, Berlin, pp 291–345.
25. Rasband WS, Bright DS 1995 NIH Image: A public domain image processing program for the Macintosh. Microbeam Anal Soc J **4:**137–149.
26. Fiori CE, Swyt CR 1992 NIST/NIH Desktop Spectrum Analyzer (DTSA), SRD-38, 2.5.0 ed. National Institute of Standards and Technology, Gaithersburg, MD, USA.
27. Landis WJ, Glimcher MJ 1982 Electron optical and analytical observations of rat growth plate cartilage prepared by ultracryomicrotomy: The failure to detect a mineral phase in matrix vesicles and the identification of heterodispersed particles as the initial solid phase of calcium phosphate deposited in the extracellular matrix. J Ultrastruct Res **78:**227–268.
28. Landis WJ 1979 Application of electron probe X-ray microanalysis to calcification studies of bone and cartilage. Scan Electron Microsc **2:**555–570.
29. Arsenault AL, Ottensmeyer FP 1983 Quantitative spatial distributions of calcium, phosphorus, and sulfur in calcifying epiphysis by high resolution electron spectroscopic imaging. Proc Natl Acad Sci USA **80:**1322–1326.
30. Hunter GK 1991 Role of proteoglycan in the provisional calcification of cartilage. A review and reinterpretation. Clin Orthop 256–280.
31. Landis WJ 1996 Mineral characterization in calcifying tissues: Atomic, molecular and macromolecular perspectives. Connect Tissue Res **34:**239–246.
32. Werner A, Grunder W 1999 Calcium-induced structural changes of cartilage proteoglycans studied by ^{1}H NMR relaxometry and diffusion measurements. Magn Reson Med **41:**43–50.
33. Kim DK, Ceckler TL, Hascall VC, Calabro A, Balaban RS 1993 Analysis of water-macromolecule proton magnetization transfer in articular cartilage. Magn Reson Med **29:**211–215.
34. Gray ML, Burstein D, Lesperance LM, Gehrke L 1995 Magnetization transfer in cartilage and its constituent macromolecules. Magn Reson Med **34:**319–325.
35. Tenner MS, Spiller M, Koenig SH, Valsamis MP, Childress S, Brown RD, third, Kasoff SS 1995 Calcification can shorten T2, but not T1, at magnetic resonance imaging fields. Results of a relaxometry study of calcified human meningiomas. Invest Radiol **30:**345–353.
36. Davis CA, Genant HK, Dunham JS 1986 The effects of bone on proton NMR relaxation times of surrounding liquids. Invest Radiol **21:**472–477.
37. Henkelman RM, Watts JF, Kucharczyk W 1991 High signal intensity in MR images of calcified brain tissue. Radiology **179:**199–206.
38. Anderson HC 1989 Mechanism of mineral formation in bone. Lab Invest **60:**320–330.

Address reprint requests to:
Kimberlee Potter, Ph.D.
Department of Cellular Pathology and Genetics
Armed Forces Institute of Pathology Annex
1413 Research Boulevard, Building 101, Room 1008
Rockville, MD 20850, USA

Received in original form June 30, 2001; in revised form September 19, 2001; accepted October 22, 2001.